Smart Mater. Struct. 18 (2009) 065015 (12pp) doi:10.1088/0964-1726/18/6/065015

An edge-based smoothed finite element method for analysis of two-dimensional piezoelectric structures

H Nguyen-Xuan[1,2,4], G R Liu[1,3], T Nguyen-Thoi[2,3] and C Nguyen-Tran[2]

[1] Singapore-MIT Alliance (SMA), E4-04-10, 4 Engineering Drive 3, 117576, Singapore
[2] Department of Mechanics, Faculty of Mathematics and Computer Science, University of Science, Ho Chi Minh City, Vietnam
[3] Center for Advanced Computations in Engineering Science (ACES), Department of Mechanical Engineering, National University of Singapore, 9 Engineering Drive 1, 117576, Singapore

E-mail: smanxh@nus.edu.sg and nxhung@hcmuns.edu.vn

Received 16 September 2008, in final form 31 March 2009
Published 6 May 2009
Online at stacks.iop.org/SMS/18/065015

Abstract

An edge-based smoothed finite element method (ES-FEM) was recently proposed to significantly improve the accuracy and convergence rate of the standard finite element method for static, free and forced vibration analyses of solids using three-node triangular elements that can be generated automatically for complicated geometries. In this work, it is further extended to static and eigenvalue analyses of two-dimensional piezoelectric structures. In the present ES-FEM, the approximation of the displacement and electric potential fields is the same as in the standard linear FEM, while mechanical strains and electric fields are smoothed over the smoothing domains associated with the edges of the triangles. The system stiffness matrix is then computed via a simple summation over these smoothed domains. The results of several numerical examples show that: (1) the ES-FEM is in a good agreement with the analytical solutions as well as experimental ones and (2) the ES-FEM is much more accurate than the linear triangular elements (T3) and often found to be even more accurate than the FEM using quadrilateral elements (Q4) when the same sets of nodes are used.

(Some figures in this article are in colour only in the electronic version)

1. Introduction

Piezoelectric materials have been widely used in various applications such as automotive sensors, actuators, transducers and active damping devices. One of the essential features of piezoelectric materials is the ability of transformation between mechanical energy and electric energy. Due to this attractive feature, piezoelectric materials are often used to design smart structures in industrial, medical, military and scientific areas. Because of limitations of the analytical solutions for solving practical problems of complicated geometry, the finite element method (FEM) has become the most popular numerical tool for analyzing and designing piezoelectric structures, see the literature survey in [1]. Inheriting the work of Allik and Hughes [2] for piezoelectric analysis using the FEM, most of the finite element models use only displacement and electric potentials which satisfy fully the compatibility conditions. However, these elements are often found to be less accurate and sensitive to a distortion mesh due to the overestimation of the stiffness matrix. To avoid these drawbacks, many finite element models have been proposed to improve the standard finite elements such as the bubble/incompatible displacement method [3], mixed and hybrid formulations [4–9] and development of the piezoelectric finite element with drilling degrees of freedom [10–13]. Several meshless methods have also been used to analyze piezoelectric structures such as the meshless point collocation method (PCM) [14], the point interpolation method (PIM) [15] and the radial point interpolation method (RPIM) [16].

[4] Author to whom any correspondence should be addressed.

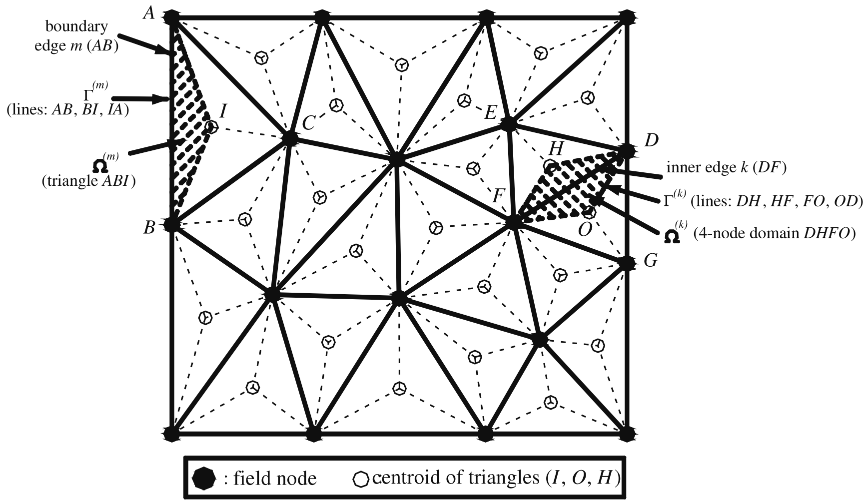

Figure 1. Division of domain into triangular element and smoothing cells $\Omega^{(k)}$ connected to edge k of triangular elements.

On the other front in the development of numerical methods, Liu *et al* [17–19] have formulated a cell/element-based smoothed finite element method (CS-FEM or SFEM) for 2D elasticity by combining a strain smoothing technique [20] with the standard finite element method. The CS-FEM has also been developed for general n-sided polygonal elements (nCS-FEM or nSFEM) [21], dynamic analyses [22] and further extended for plate and shell analyses [23, 24] and piezoelectric structures [25]. Based on the idea of CS-FEM, a node-based smoothed finite element method (NS-FEM) [26] for 2D solid mechanics problems has been developed. In the NS-FEM, the elements used can be triangles or n-sided polygons and a simple average interpolation technique is used to create the shape functions or the assumed displacement field [21]. The stiffness matrix is computed using smoothed strains over smoothing domains associated with field nodes.

It was shown that NS-FEM works well for locking problems and achieves a much more accurate stress solution when triangular elements are used. Furthermore, NS-FEM can provide an upper bound [26] to the exact solution in the strain energy for elasticity problems with non-zero external forces. However, it is also observed that NS-FEM can lead to spurious non-zero energy modes for dynamic problems. This shortcoming is due to the ‘overly-soft’ behavior that is in contrast to the ‘overly-stiff’ phenomenon of the compatible FEM (T3). To overcome this problem, an edge-based smoothed finite element method (ES-FEM) [27] has been recently developed for static, free and forced vibration analyses in 2D solid mechanics problems. The ES-FEM uses triangular elements that can be generated automatically for complicated domains and be applied widely to practical problems. In the ES-FEM, the system stiffness matrix is computed using strains smoothed over the smoothing domains associated with the edges of the triangles. For triangular elements, the smoothing domain $\Omega^{(k)}$ associated with the edge k is created by connecting two end points of the edge to the centroids of the adjacent elements as shown in figure 1. It has been demonstrated in [27] that the ES-FEM using triangular meshes is always stable, efficient and often found to be even more accurate than the standard FEM using quadrilateral elements (Q4) without adding any additional degrees of freedom. The ES-FEM has also been extended to the so-called face-based finite element method (FS-FEM) [28] for solving 3D linear and nonlinear solid mechanics problems.

This paper further extends the ES-FEM to static and frequency analyses of piezoelectric structures. Three-node triangular elements with only linear shape functions are used and the problem domain is subdivided into the union of smoothing domains associated with the edges of triangles. Smoothed strains and smoothed electrics are obtained by applying the gradient smoothing technique over the edge-based smoothing domains. Because the ES-FEM uses the linear shape functions and the constant smoothing operation, the computation of the stiffness matrix becomes a simple summation over these smoothing domains. Some numerical examples are analyzed to demonstrate the accuracy, stability and effectiveness of the ES-FEM by comparing with the results of the standard FEM, the analytical solutions as well as experimental ones.

2. The Galerkin weak form and finite element formulation for the piezoelectric problem

In this section, a finite element formulation for piezoelectricity is established via a variational formulation [1, 2]. Consider a piezoelectric solid occupying a two-dimensional space with domain Ω bounded by Γ; the following general energy functional L is used to express a summation of kinetic energy, strain energy, dielectric energy and external work:

$$L = \int_{\Omega} \left[\tfrac{1}{2}\rho\dot{\mathbf{u}}^{\mathrm{T}}\dot{\mathbf{u}} - \tfrac{1}{2}\mathbf{S}^{\mathrm{T}}\mathbf{T} + \tfrac{1}{2}\mathbf{D}^{\mathrm{T}}\mathbf{E} + \mathbf{u}^{\mathrm{T}}\mathbf{f}_{\mathrm{s}} - \boldsymbol{\phi}\mathbf{q}_{\mathrm{s}}\right] \mathrm{d}\Omega + \sum \mathbf{u}^{\mathrm{T}}\mathbf{F}_{\mathrm{p}} - \sum \boldsymbol{\phi}\mathbf{Q}_{\mathrm{p}} \quad (1)$$

where $\mathbf{u}$ and $\dot{\mathbf{u}}$ are the vectors of mechanical displacement and mechanical velocity; $\boldsymbol{\phi}$ denotes the electric potential vector; $\mathbf{T}$ and $\mathbf{S}$ are the stress and strain vectors; $\mathbf{D}$ and $\mathbf{E}$ are dielectric displacement and electric field vectors; $\mathbf{f}_{\mathrm{s}}$ and $\mathbf{F}_{\mathrm{p}}$ denote the vectors of the mechanical surface loads and point loads; and $\mathbf{q}_s$ and $\mathbf{Q}_p$ denote the vectors of surface charges and point charges.

For the linear electroelastic problem, the constitutive equations have the following form:

$$\begin{bmatrix} \mathbf{T} \\ \mathbf{D} \end{bmatrix} = \begin{bmatrix} \mathbf{c}_E & -\mathbf{e}^{\mathrm{T}} \\ \mathbf{e} & \boldsymbol{\varepsilon}_S \end{bmatrix} \begin{bmatrix} \mathbf{S} \\ \mathbf{E} \end{bmatrix} \tag{2}$$

where $\mathbf{c}_E$ denotes the elastic matrix measured at constant electric field, $\boldsymbol{\varepsilon}_S$ is the dielectric matrix at constant mechanical strain and $\mathbf{e}$ is the piezoelectric matrix.

The strain–displacement and electric field–potential relationships are expressed by

$$\mathbf{S} = \nabla_s \mathbf{u} \tag{3}$$

$$\mathbf{E} = -\mathrm{grad}\,\phi \tag{4}$$

where ∇_s is the symmetric gradient operator:

$$\nabla_s = \begin{bmatrix} \frac{\partial}{\partial x} & 0 & \frac{\partial}{\partial y} \\ 0 & \frac{\partial}{\partial y} & \frac{\partial}{\partial x} \end{bmatrix}^{\mathrm{T}}. \tag{5}$$

To obtain approximate solutions for piezoelectricity, the standard three-node triangular element (T3) is used. The finite element approximation is expressed as

$$\mathbf{u}(\mathbf{x}) = \sum_{I=1}^{np} \begin{bmatrix} N_I(\mathbf{x}) & 0 \\ 0 & N_I(\mathbf{x}) \end{bmatrix} \mathbf{d}_I, \qquad \phi(\mathbf{x}) = \sum_{I=1}^{np} N_I(\mathbf{x})\phi_I \tag{6}$$

where np is the total number of nodes in the problem domains, $\mathbf{d}_I = [u_I \quad v_I]^{\mathrm{T}}$ are the nodal degrees of freedom of $\mathbf{u} = [u \quad v]^{\mathrm{T}}$ associated with node I and $N_I(\mathbf{x})$ is the linear shape functions of triangular elements. Substituting the approximations (6) into equations (3) and (4), we obtain

$$\mathbf{S} = \nabla_s \mathbf{u} = \sum_{I=1}^{np} \mathbf{B}_{uI} \mathbf{d}_I \tag{7}$$

$$\mathbf{E} = -\mathrm{grad}\,\phi = -\sum_{I=1}^{np} \mathbf{B}_{\phi I} \phi_I \tag{8}$$

where

$$\mathbf{B}_{uI} = \begin{bmatrix} N_{I,x} & 0 \\ 0 & N_{I,y} \\ N_{I,y} & N_{I,x} \end{bmatrix}, \qquad \mathbf{B}_{\phi I} = \begin{bmatrix} N_{I,x} \\ N_{I,y} \end{bmatrix}. \tag{9}$$

By taking Hamilton's variational principle:

$$\delta \int_{t_1}^{t_2} L\,\mathrm{d}t = 0 \tag{10}$$

and then substituting equations (6)–(8) into (10), we have a set of piezoelectric dynamic equations:

$$\begin{bmatrix} \mathbf{m} & \mathbf{0} \\ \mathbf{0} & \mathbf{0} \end{bmatrix} \begin{Bmatrix} \ddot{\mathbf{d}} \\ \ddot{\boldsymbol{\Phi}} \end{Bmatrix} + \begin{bmatrix} \mathbf{k}_{uu} & \mathbf{k}_{u\phi} \\ \mathbf{k}_{u\phi}^{\mathrm{T}} & \mathbf{k}_{\phi\phi} \end{bmatrix} \begin{Bmatrix} \mathbf{d} \\ \boldsymbol{\Phi} \end{Bmatrix} = \begin{Bmatrix} \mathbf{F} \\ \mathbf{Q} \end{Bmatrix} \tag{11}$$

where

$$\mathbf{m} = \int_\Omega \rho \mathbf{N}_u^{\mathrm{T}} \mathbf{N}_u \,\mathrm{d}\Omega \tag{12}$$

$$\mathbf{k}_{uu} = \int_\Omega \mathbf{B}_u^{\mathrm{T}} c_E \mathbf{B}_u \,\mathrm{d}\Omega \tag{13}$$

$$\mathbf{k}_{u\phi} = \int_\Omega \mathbf{B}_u^{\mathrm{T}} \mathbf{e}^{\mathrm{T}} \mathbf{B}_\phi \,\mathrm{d}\Omega \tag{14}$$

$$\mathbf{k}_{\phi\phi} = -\int_\Omega \mathbf{B}_\phi^{\mathrm{T}} \boldsymbol{\varepsilon}_S \mathbf{B}_\phi \,\mathrm{d}\Omega \tag{15}$$

$$\mathbf{F} = \int_\Omega \mathbf{N}_u^{\mathrm{T}} \mathbf{f}_s \,\mathrm{d}\Omega + \mathbf{N}_u^{\mathrm{T}} \mathbf{F}_p \tag{16}$$

$$\mathbf{Q} = -\int_\Omega \mathbf{N}_\phi^{\mathrm{T}} \mathbf{q}_s \,\mathrm{d}\Omega - \mathbf{N}_\phi^{\mathrm{T}} \mathbf{Q}_p. \tag{17}$$

Note that equations (12)–(15) are used only for plane stress/strain problems. For axisymmetric problems, these derivatives shall have the following form:

$$\mathbf{B}_{uI} = \begin{bmatrix} N_{I,r} & 0 \\ \frac{N_I}{r} & 0 \\ 0 & N_{I,z} \\ N_{I,z} & N_{I,r} \end{bmatrix}, \qquad \mathbf{B}_{\phi I} = \begin{bmatrix} N_{I,r} \\ \frac{N_I}{r} \\ N_{I,z} \end{bmatrix}. \tag{18}$$

3. An edge-based smoothed finite element method for the piezoelectric problem

The above equations are the basic form for analyses of piezoelectric solids using the standard FEM. Similar to the FEM, the ES-FEM also uses a mesh of elements. When three-node triangular elements are used, the shape functions used in the ES-FEM are also identical to those in the FEM and hence the displacement field in the ES-FEM is also ensured to be continuous on the whole problem domain.

3.1. A smoothing operator on mechanical strains and electric field

In the ES-FEM, we do not use the compatible strain fields (3) but strains 'smoothed' over local smoothing domains, and naturally the integration for the stiffness matrix $\mathbf{K}$ is no longer based on elements, but on these smoothing domains. These local smoothing domains are constructed based on edges of the elements such that $\Omega = \cup_{k=1}^{N_e} \Omega^{(k)}$ and $\Omega^{(i)} \cap \Omega^{(j)} = \emptyset$ for $i \neq j$, in which N_e is the total number of edges of all elements in the entire problem domain. For triangular elements, the smoothing domain $\Omega^{(k)}$ associated with the edge k is created by connecting two end points of the edge to centroids of adjacent elements as shown in figure 1.

Using the edge-based smoothing domains, smoothed strains and smoothed electric fields over a smoothing domain $\Omega^{(k)}$ associated with edge k are constructed by smoothing the compatible strains and electric fields as

$$\tilde{\mathbf{S}} = \int_{\Omega^{(k)}} \mathbf{S}(\mathbf{x}) \Phi^{(k)}(\mathbf{x}) \,\mathrm{d}\Omega \tag{19}$$

$$\tilde{\mathbf{E}} = \int_{\Omega^{(k)}} \mathbf{E}(\mathbf{x}) \Phi^{(k)}(\mathbf{x}) \,\mathrm{d}\Omega \tag{20}$$

where $\Phi^{(k)}(\mathbf{x})$ is simply chosen to be a step function:

$$\Phi^{(k)}(\mathbf{x}) = \begin{cases} 1/A^{(k)} & \mathbf{x} \in \Omega^{(k)} \\ 0 & \mathbf{x} \notin \Omega^{(k)} \end{cases} \tag{21}$$

where $A^{(k)}$ is the area of the smoothing domain $\Omega^{(k)}$:

$$A^{(k)} = \int_{\Omega^{(k)}} \mathrm{d}\Omega = \tfrac{1}{3}\sum_{j=1}^{N_{\mathrm{e}}^{(k)}} A_{\mathrm{e}}^{(j)} \tag{22}$$

where $N_{\mathrm{e}}^{(k)}$ is the total number of elements around the edge k ($N_{\mathrm{e}}^{(k)} = 1$ for the boundary edges and $N_{\mathrm{e}}^{(k)} = 2$ for the inner edges as shown in figure 1) and $A_{\mathrm{e}}^{(j)}$ is the area of the jth element sharing edge k.

Substituting equation (21) into equations (19) and (20) and applying the divergence theorem, the smoothed strains and smoothed electric fields become

$$\begin{aligned}\tilde{\mathbf{S}} &= \frac{1}{A^{(k)}}\int_{\Omega^{(k)}} \mathbf{S}(\mathbf{x})\,\mathrm{d}\Omega = \frac{1}{A^{(k)}}\int_{\Omega^{(k)}} \nabla_{\mathrm{s}}\mathbf{u}(\mathbf{x})\,\mathrm{d}\Omega \\ &= \frac{1}{A^{(k)}}\int_{\Gamma^{(k)}} \mathbf{n}_u^{(k)}(\mathbf{x})\mathbf{u}(\mathbf{x})\,\mathrm{d}\Gamma \end{aligned} \tag{23}$$

$$\begin{aligned}\tilde{\mathbf{E}} &= \frac{1}{A^{(k)}}\int_{\Omega^{(k)}} \mathbf{E}(\mathbf{x})\,\mathrm{d}\Omega = -\frac{1}{A^{(k)}}\int_{\Omega^{(k)}} \mathrm{grad}\,\phi(\mathbf{x})\,\mathrm{d}\Omega \\ &= -\frac{1}{A^{(k)}}\int_{\Gamma^{(k)}} \mathbf{n}_\phi^{(k)}(\mathbf{x})\phi(\mathbf{x})\,\mathrm{d}\Gamma \end{aligned} \tag{24}$$

where $\Gamma^{(k)}$ is the boundary of the smoothing domain $\Omega^{(k)}$, and $\mathbf{n}_u^{(k)}$ and $\mathbf{n}_\phi^{(k)}$ are the outward normal matrices on the boundary $\Gamma^{(k)}$ defined by

$$\mathbf{n}_u^{(k)}(\mathbf{x}) = \begin{bmatrix} n_x^{(k)} & 0 \\ 0 & n_y^{(k)} \\ n_y^{(k)} & n_x^{(k)} \end{bmatrix}, \qquad \mathbf{n}_\phi^{(k)}(\mathbf{x}) = [\,n_x^{(k)} \quad n_y^{(k)}\,]^{\mathrm{T}}. \tag{25}$$

Therefore the vectors of mechanical stresses and dielectric displacements can be modified to the following formulation:

$$\begin{bmatrix} \tilde{\mathbf{T}} \\ \tilde{\mathbf{D}} \end{bmatrix} = \begin{bmatrix} \mathbf{c}_E & -\mathbf{e}^{\mathrm{T}} \\ \mathbf{e} & \boldsymbol{\varepsilon}_S \end{bmatrix} \begin{bmatrix} \tilde{\mathbf{S}} \\ \tilde{\mathbf{E}} \end{bmatrix}. \tag{26}$$

3.2. Smoothed stiffness matrices for piezoelectricity problems

We now introduce two simple ways to compute smoothed matrices in the ES-FEM. By substituting equation (6) into equations (21)–(23), the smoothed strain and the smoothed electric field on the domain $\Omega^{(k)}$ sharing edge k can be written in the following matrix form of nodal variables:

$$\tilde{\mathbf{S}} = \frac{1}{A^{(k)}}\int_{\Omega^{(k)}} \nabla_{\mathrm{s}}\mathbf{u}(\mathbf{x})\,\mathrm{d}\Omega = \sum_{I\in N_{\mathrm{n}}^{(k)}} \tilde{\mathbf{B}}_{uI}^{(k)}(\mathbf{x}_k)\mathbf{d}_I \tag{27}$$

$$\tilde{\mathbf{E}} = -\frac{1}{A^{(k)}}\int_{\Omega^{(k)}} \mathrm{grad}\,\phi(\mathbf{x})\,\mathrm{d}\Omega = -\sum_{I\in N_{\mathrm{n}}^{(k)}} \tilde{\mathbf{B}}_{\phi I}^{(k)}(\mathbf{x}_k)\phi_I \tag{28}$$

where $N_{\mathrm{n}}^{(k)}$ is the set of nodes of the elements having the common edge k (for example, $N_{\mathrm{n}}^{(k)} = \{A,\ B,\ C\}$ for boundary edge m and $N_{\mathrm{n}}^{(k)} = \{D,\ E,\ F,\ G\}$ for inner edge k as shown in figure 1); $\tilde{\mathbf{B}}_{uI}^{(k)}(\mathbf{x}_k)$ and $\tilde{\mathbf{B}}_{\phi I}^{(k)}(\mathbf{x}_k)$ are termed the smoothed strain and electric matrices on the smoothing domain $\Omega^{(k)}$ for plane stress/strain problems, and calculated explicitly by an assembly process similar to that in the FEM:

$$\begin{aligned}\tilde{\mathbf{B}}_{uI}^{(k)}(\mathbf{x}_k) &= \frac{1}{A^{(k)}}\sum_{j=1}^{N_{\mathrm{e}}^{(k)}} \frac{1}{3}A_j^{\mathrm{e}}\mathbf{B}_{uj}, \\ \tilde{\mathbf{B}}_{\phi I}^{(k)}(\mathbf{x}_k) &= \frac{1}{A^{(k)}}\sum_{j=1}^{N_{\mathrm{e}}^{(k)}} \frac{1}{3}A_j^{\mathrm{e}}\mathbf{B}_{\phi j}\end{aligned} \tag{29}$$

where $\mathbf{B}_{uj}$, $\mathbf{B}_{\phi j}$ are the constant strain gradient matrices of the jth element around the edge k when the triangular elements with linear shape functions are used. Note that the matrices in equations (29) are directly constructed from the area and the usual 'compatible' strain matrices of the standard FEM using triangular elements. However, these formulations are only suitable for approximations with the constant compatible strain matrices such as three-node triangular elements for 2D problems and four-node tetrahedral elements for 3D problems. Therefore, to obtain a general way that can work well for n-sided polygonal elements, the smoothed strains and smoothed electric fields should now be computed along the boundary of the smoothing domains (cf equations (23) and (24)) as

$$\tilde{\mathbf{S}} = \frac{1}{A^{(k)}}\int_{\Gamma^{(k)}} \mathbf{n}_u^{(k)}\mathbf{u}(\mathbf{x})\,\mathrm{d}\Gamma = \sum_{I\in N_{\mathrm{n}}^{(k)}} \tilde{\mathbf{B}}_{uI}^{(k)}(\mathbf{x}_k)\mathbf{d}_I \tag{30}$$

$$\tilde{\mathbf{E}} = -\frac{1}{A^{(k)}}\int_{\Omega^{(k)}} \mathrm{grad}\,\phi(\mathbf{x})\,\mathrm{d}\Omega = -\sum_{I\in N_{\mathrm{n}}^{(k)}} \tilde{\mathbf{B}}_{\phi}^{(k)}(\mathbf{x}_k)\phi_I \tag{31}$$

where $\tilde{\mathbf{B}}_{uI}^{(k)}$ and $\tilde{\mathbf{B}}_{\phi I}^{(k)}$ are computed by the following formulations:

$$\tilde{\mathbf{B}}_{uI}^{(k)} = \frac{1}{A^{(k)}}\begin{bmatrix} \int_{\Gamma^{(k)}} N_I(\mathbf{x})n_x^{(k)}\,\mathrm{d}\Gamma & 0 \\ 0 & \int_{\Gamma^{(k)}} N_I(\mathbf{x})n_y^{(k)}\,\mathrm{d}\Gamma \\ \int_{\Gamma^{(k)}} N_I(\mathbf{x})n_y^{(k)}\,\mathrm{d}\Gamma & \int_{\Gamma^{(k)}} N_I(\mathbf{x})n_x^{(k)}\,\mathrm{d}\Gamma \end{bmatrix} \tag{32}$$

$$\tilde{\mathbf{B}}_{\phi I}^{(k)} = \frac{1}{A^{(k)}}\begin{bmatrix} \int_{\Gamma^{(k)}} N_I(\mathbf{x})n_x^{(k)}\,\mathrm{d}\Gamma \\ \int_{\Gamma^{(k)}} N_I(\mathbf{x})n_y^{(k)}\,\mathrm{d}\Gamma \end{bmatrix}. \tag{33}$$

Next, let the boundary $\Gamma^{(k)}$ of an arbitrary smoothing domain $\Omega^{(k)}$ be the sum of the boundary segments $\Gamma_b^{(k)}$, $\Gamma^{(k)} = \cup_{b=1}^{nb}\Gamma_b^{(k)}$, where nb is the total number of the boundary segments of $\Gamma^{(k)}$, for example $nb = 3$ (AB, BI, IA) for boundary edge m and $nb = 4$ (FO, OD, DH, HF) for inner edge k as shown in figure 1. Using the linear shape function of triangles as in the FEM, the displacement field in the ES-FEM is linear compatible along the boundary $\Gamma^{(k)}$. Therefore, one Gaussian point is sufficient for the accurate line integration along each segment of boundary $\Gamma_b^{(k)}$ of $\Gamma^{(k)}$. Hence the above equation can be further simplified to its algebraic form:

$$\begin{aligned}\tilde{\mathbf{B}}_{uI}^{(k)} &= \frac{1}{A^{(k)}}\begin{bmatrix} \int_{\Gamma^{(k)}} N_I n_x\,\mathrm{d}\Gamma & 0 \\ 0 & \int_{\Gamma^{(k)}} N_I n_y\,\mathrm{d}\Gamma \\ \int_{\Gamma^{(k)}} N_I n_y\,\mathrm{d}\Gamma & \int_{\Gamma^{(k)}} N_I n_x\,\mathrm{d}\Gamma \end{bmatrix} \\ &= \frac{1}{A^{(k)}}\sum_{b=1}^{nb}\begin{bmatrix} N_I(\mathbf{x}_b^{\mathrm{G}})n_x^{(k)}(\mathbf{x}_b^{\mathrm{G}}) & 0 \\ 0 & N_I(\mathbf{x}_b^{\mathrm{G}})n_y^{(k)}(\mathbf{x}_b^{\mathrm{G}}) \\ N_I(\mathbf{x}_b^{\mathrm{G}})n_y^{(k)}(\mathbf{x}_b^{\mathrm{G}}) & N_I(\mathbf{x}_b^{\mathrm{G}})n_x^{(k)}(\mathbf{x}_b^{\mathrm{G}}) \end{bmatrix} l_b^{(k)}\end{aligned} \tag{34}$$

$$\tilde{\mathbf{B}}_{\phi I}^{(k)} = \frac{1}{A^{(k)}}\begin{bmatrix}\int_{\Gamma^{(k)}} N_I n_x\,\mathrm{d}\Gamma \\ \int_{\Gamma^{(k)}} N_I n_y\,\mathrm{d}\Gamma\end{bmatrix} = \frac{1}{A^{(k)}}\sum_{b=1}^{nb}\begin{bmatrix}N_I(\mathbf{x}_b^{\mathrm{G}})n_x^{(k)}(\mathbf{x}_b^{\mathrm{G}}) \\ N_I(\mathbf{x}_b^{\mathrm{G}})n_y^{(k)}(\mathbf{x}_b^{\mathrm{G}})\end{bmatrix} l_b^{(k)} \tag{35}$$

where $\mathbf{x}_b^{\mathrm{G}}$ and $l_b^{(k)}$ are the midpoint (Gauss point) and the length of $\Gamma_b^{(k)}$, respectively.

Equations (34) and (35) imply that no derivative of shape functions is used in computing the gradients and only FEM shape function values at some particular points along the segments of the smoothing domain boundary are required.

For axisymmetric problems, the smoothed strain and electric matrices are computed as

$$\tilde{\mathbf{B}}_{uI}^{(k)} = \begin{bmatrix}\frac{1}{A^{(k)}}\int_{\Gamma^{(k)}} N_I(\mathbf{x})n_r^{(k)}(\mathbf{x})\,\mathrm{d}\Gamma & 0 \\ \frac{N_I(\mathbf{x})}{r} & 0 \\ 0 & \frac{1}{A^{(k)}}\int_{\Gamma^{(k)}} N_I(\mathbf{x})n_z^{(k)}(\mathbf{x})\,\mathrm{d}\Gamma \\ \frac{1}{A^{(k)}}\int_{\Gamma^{(k)}} N_I(\mathbf{x})n_r^{(k)}(\mathbf{x})\,\mathrm{d}\Gamma & \frac{1}{A^{(k)}}\int_{\Gamma^{(k)}} N_I(\mathbf{x})n_r^{(k)}(\mathbf{x})\,\mathrm{d}\Gamma\end{bmatrix}$$

$$= \begin{bmatrix}\frac{1}{A^{(k)}}\sum_{b=1}^{nb} N_I(\mathbf{x}_b^{\mathrm{G}})n_r^{(k)}(\mathbf{x}_b^{\mathrm{G}})l_b^{(k)} & 0 \\ \frac{1}{r^{(k)}}\frac{\sum_{b=1}^{nb} N_I(\mathbf{x}_b^{\mathrm{G}})}{nb} & 0 \\ 0 & \frac{1}{A^{(k)}}\sum_{b=1}^{nb} N_I(\mathbf{x}_b^{\mathrm{G}})n_z^{(k)}(\mathbf{x}_b^{\mathrm{G}})l_b^{(k)} \\ \frac{1}{A^{(k)}}\sum_{b=1}^{nb} N_I(\mathbf{x}_b^{\mathrm{G}})n_z^{(k)}(\mathbf{x}_b^{\mathrm{G}})l_b^{(k)} & \frac{1}{A^{(k)}}\sum_{b=1}^{nb} N_I(\mathbf{x}_b^{\mathrm{G}})n_r^{(k)}(\mathbf{x}_b^{\mathrm{G}})l_b^{(k)}\end{bmatrix} \tag{36}$$

$$\tilde{\mathbf{B}}_{\phi I}^{(k)} = \begin{bmatrix}\frac{1}{A^{(k)}}\int_{\Gamma^{(k)}} N_I(\mathbf{x})n_r^{(k)}(\mathbf{x})\,\mathrm{d}\Gamma \\ \frac{N_I(\mathbf{x})}{r} \\ \frac{1}{A^{(k)}}\int_{\Gamma^{(k)}} N_I(\mathbf{x})n_z^{(k)}(\mathbf{x})\,\mathrm{d}\Gamma\end{bmatrix} = \begin{bmatrix}\frac{1}{A^{(k)}}\sum_{b=1}^{nb} N_I(\mathbf{x}_b^{(k)})n_r^{(k)}(\mathbf{x}_b^{(k)})l_b^{(k)} \\ \frac{1}{r^{(k)}}\frac{\sum_{b=1}^{nb} N_I(\mathbf{x}_b^{(k)})}{nb} \\ \frac{1}{A^{(k)}}\sum_{b=1}^{nb} N_I(\mathbf{x}_b^{(k)})n_z^{(k)}(\mathbf{x}_b^{(k)})l_b^{(k)}\end{bmatrix} \tag{37}$$

where $r^{(k)}$ is determined at the midpoint of edge k.

A linear equations system is then obtained:

$$\begin{bmatrix}\mathbf{m} & \mathbf{0} \\ \mathbf{0} & \mathbf{0}\end{bmatrix}\begin{Bmatrix}\ddot{\mathbf{d}} \\ \ddot{\mathbf{\Phi}}\end{Bmatrix} + \begin{bmatrix}\tilde{\mathbf{k}}_{uu} & \tilde{\mathbf{k}}_{u\phi} \\ \tilde{\mathbf{k}}_{u\phi}^{\mathrm{T}} & \tilde{\mathbf{k}}_{\phi\phi}\end{bmatrix}\begin{Bmatrix}\mathbf{d} \\ \mathbf{\Phi}\end{Bmatrix} = \begin{Bmatrix}\mathbf{F} \\ \mathbf{Q}\end{Bmatrix} \tag{38}$$

where

$$\tilde{\mathbf{k}}_{uu} = \sum_{k\in N_e}\int_{\Omega^{(k)}} (\tilde{\mathbf{B}}_u^{(k)})^{\mathrm{T}}\mathbf{c}_E\tilde{\mathbf{B}}_u^{(k)}\,\mathrm{d}\Omega = \sum_{k\in N_e}(\tilde{\mathbf{B}}_u^{(k)})^{\mathrm{T}}\mathbf{c}_E\tilde{\mathbf{B}}_u^{(k)}A^{(k)} \tag{39}$$

$$\tilde{\mathbf{k}}_{u\phi} = \sum_{k\in N_e}\int_{\Omega^{(k)}} (\tilde{\mathbf{B}}_u^{(k)})^{\mathrm{T}}\mathbf{e}^{\mathrm{T}}\tilde{\mathbf{B}}_\phi^{(k)}\,\mathrm{d}\Omega = \sum_{k\in N_e}(\tilde{\mathbf{B}}_u^{(k)})^{\mathrm{T}}\mathbf{e}^{\mathrm{T}}\tilde{\mathbf{B}}_\phi^{(k)}A^{(k)} \tag{40}$$

$$\tilde{\mathbf{k}}_{\phi\phi} = -\sum_{k\in N_e}\int_{\Omega^{(k)}} (\tilde{\mathbf{B}}_\phi^{(k)})^{\mathrm{T}}\boldsymbol{\varepsilon}_S\tilde{\mathbf{B}}_\phi^{(k)}\,\mathrm{d}\Omega = -\sum_{k\in N_e}(\tilde{\mathbf{B}}_\phi^{(k)})^{\mathrm{T}}\boldsymbol{\varepsilon}_S\tilde{\mathbf{B}}_\phi^{(k)}A^{(k)}. \tag{41}$$

Equations (39)–(41) give a simple way to compute the stiffness matrices of smoothing domains associated with edges of the elements. Finally, we note that the trial functions $\mathbf{u}(\mathbf{x})$, $\phi(\mathbf{x})$ are the same as those given in equation (6), and therefore the force vector $\mathbf{F}$, $\mathbf{Q}$ and mass matrix $\mathbf{m}$ in the ES-FEM are also calculated in the same way as in the FEM. In other words, the ES-FEM changes only the stiffness matrix.

4. Numerical results

In this section, benchmark problems are examined for the piezoelectric ES-FEM. For comparison, the elements used in this paper are denoted as follows:

- Q4—the standard four-node quadrilateral element using 2×2 Gauss points (FEM-Q4).
- T3—the standard three-node element with shape linear function (FEM-T3).
- ES-T3—the edge-based SFEM [27] that is found to be the 'most' accurate model using triangular elements (ES-FEM-T3) so far.

The PVDF, PZT4 and PZT5 materials are used and their features are referred to by

- PZT4 [9]

$$c_{11} = 139\times 10^3,\qquad c_{33} = 113\times 10^3,$$

$$c_{13} = 74.3\times 10^3,\qquad c_{55} = 25.6\times 10^3\ (\mathrm{N\ mm^{-2}})$$

$$e_{15} = 13.44\times 10^6,\qquad e_{31} = -6.98\times 10^6,$$

$$e_{33} = 13.84\times 10^6\ (\mathrm{pC\ mm^{-2}})$$

$$\varepsilon_{11} = 6.00\times 10^9,\qquad \varepsilon_{33} = 5.47\times 10^9\ (\mathrm{pC\ GV^{-1}\ mm^{-1}})$$

- PVDF [14]

$$c_{11} = 2.18\times 10^{-3},\qquad c_{13} = 6.33\times 10^{-4},$$

$$c_{33} = 2.18\times 10^{-3},\qquad c_{55} = 7.75\times 10^{-4}\ (\mathrm{N\ \mu m^{-2}})$$

$$e_{31} = e_{33} = 4.6\times 10^{-8}\ (\mathrm{N\ V^{-1}\ \mu m^{-1}})$$

$$\varepsilon_{11} = \varepsilon_{33} = 1.062\times 10^{-10}\ (\mathrm{N\ V^{-2}})$$

- PZT5 [14]

$$s_{11} = 16.4\times 10^{-6},\qquad s_{13} = -7.22\times 10^{-6},$$

$$s_{33} = 18.8\times 10^{-6},\qquad s_{55} = 47.5\times 10^{-6}\ (\mathrm{mm^2\ N^{-1}})$$

$$d_{31} = -172\times 10^{-9},\qquad d_{33} = 374\times 10^{-9},$$

$$d_{15} = 584\times 10^{-9}\ (\mathrm{mm\ V^{-1}})$$

$$\epsilon_{11} = 1.531\,05\times 10^{-8},\qquad \epsilon_{33} = 1.505\times 10^{-7}\ (\mathrm{N\ V^{-2}}).$$

Table 1. The results of patch test.

	Results	
Variable	Exact	ES-T3
u	$2.376\,547\,556\,249\,814 \times 10^{-6}$	$2.376\,547\,556\,249\,648 \times 10^{-6}$
v	$-1.818\,789\,953\,339\,896 \times 10^{-7}$	$-1.818\,789\,953\,339\,893 \times 10^{-7}$
ϕ	$-1.066\,703\,050\,081\,747 \times 10^{-9}$	$-1.066\,703\,050\,081\,748 \times 10^{-9}$
T_{xx}	1.0	1.0
T_{yy}	0	$-3.760\,880\,495\,917\,718 \times 10^{-15}$
T_{xy}	0	$-1.292\,368\,989\,602\,721 \times 10^{-16}$
D_x	0	$-6.039\,613\,253\,960\,852 \times 10^{-14}$
D_y	0	$3.659\,295\,089\,164\,516 \times 10^{-13}$

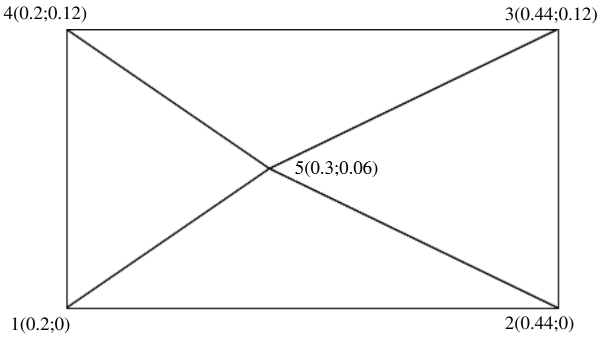

Figure 2. Patch test of piezoelectric elements.

The constant matrices $\mathbf{c}_E$, $\mathbf{e}$ and $\boldsymbol{\varepsilon}_S$ are used for the following cases:

- Plane problems:

$$\begin{bmatrix} \mathbf{c}_E & -\mathbf{e}^{\mathrm{T}} \\ \mathbf{e} & \boldsymbol{\varepsilon}_S \end{bmatrix} = \begin{bmatrix} c_{11} & c_{13} & 0 & 0 & -e_{31} \\ c_{13} & c_{33} & 0 & 0 & -e_{33} \\ 0 & 0 & c_{55} & -e_{15} & 0 \\ 0 & 0 & e_{15} & \varepsilon_{11} & 0 \\ e_{31} & e_{33} & 0 & 0 & \varepsilon_{33} \end{bmatrix}. \tag{42}$$

- Axisymmetric problems:

$$\begin{bmatrix} \mathbf{c}_E & -\mathbf{e}^{\mathrm{T}} \\ \mathbf{e} & \boldsymbol{\varepsilon}_S \end{bmatrix} = \begin{bmatrix} c_{11} & c_{12} & c_{13} & 0 & 0 & -e_{31} \\ c_{12} & c_{11} & c_{13} & 0 & 0 & -e_{31} \\ c_{13} & c_{13} & c_{33} & 0 & 0 & -e_{33} \\ 0 & 0 & 0 & c_{44} & -e_{24} & 0 \\ 0 & 0 & 0 & e_{24} & \varepsilon_{22} & 0 \\ e_{31} & e_{31} & e_{33} & 0 & 0 & \varepsilon_{33} \end{bmatrix}. \tag{43}$$

The following relations [9] are more convenient to evaluate analytical and numerical solutions:

$$\begin{bmatrix} s_{11} & s_{13} & g_{31} \\ s_{13} & s_{33} & g_{33} \\ g_{31} & g_{33} & -f_{33} \end{bmatrix} = \begin{bmatrix} c_{11} & c_{13} & e_{31} \\ c_{13} & c_{33} & e_{33} \\ e_{31} & e_{33} & -\varepsilon_{33} \end{bmatrix}^{-1} \tag{44}$$

and

$$\mathbf{d} = \mathbf{e}\mathbf{c}_E^{-1}, \qquad \boldsymbol{\varepsilon}_T = \begin{bmatrix} \epsilon_{11} & 0 \\ 0 & \epsilon_{33} \end{bmatrix}, \qquad \boldsymbol{\varepsilon}_S = \boldsymbol{\varepsilon}_T - \mathbf{e}\mathbf{c}_E^{-1}\mathbf{e}^{\mathrm{T}}. \tag{45}$$

4.1. Eigenvalues and rank

ES-T3 only contains four zero eigenvalues including the three rigid-body modes of the mechanical part and one zero eigenvalue of the constant potential field. Hence this element always has sufficient rank and no spurious zero-energy modes.

4.2. Patch test

Satisfaction of the patch test requires that a constant distribution of all quantities is reproduced for arbitrary meshes. For the piezoelectric problem, we base it on work of Sze *et al* [9] with geometry and mesh shown in figure 2. The PZT4 material is used to test this problem.

The boundary condition for mechanical displacement and electric potential is assumed to be

$$u = s_{11}\sigma_0 x, \qquad v = s_{13}\sigma_0 y, \qquad \phi = g_{31}\sigma_0 y \tag{46}$$

where σ_0 is an arbitrary stress parameter. Hence, the mechanical stresses and the dielectric displacements have the following form:

$$T_{xx} = \sigma_0, \qquad T_{xy} = T_{yy} = D_x = D_y = 0. \tag{47}$$

It is found from table 1 that all results of the ES-T3 match the exact solution within machine precision.

4.3. Singer-player piezoelectric strip

This example is to examine the accuracy of the present element under mechanical action and electric potential boundary conditions. This problem was studied previously by Ohs *et al* [14] for the performance of the meshless point collocation method. We consider the shear deformation of a 1 mm × 1 mm piezoelectric strip under the compressive stress $\sigma_0 = 5$ N mm^{-2} and an applied voltage $V_0 = 1000$ V, see figure 3. The material PZT-5 is used for this problem. The electric field is applied to the left and right edges in order to create the polarization of the material, resulting in shear strain. The mechanical and electrical boundary conditions are prescribed

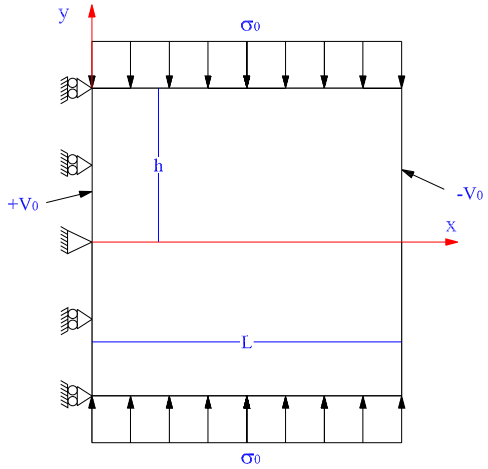

Figure 3. Piezo-strip under a uniform stress and an applied voltage.

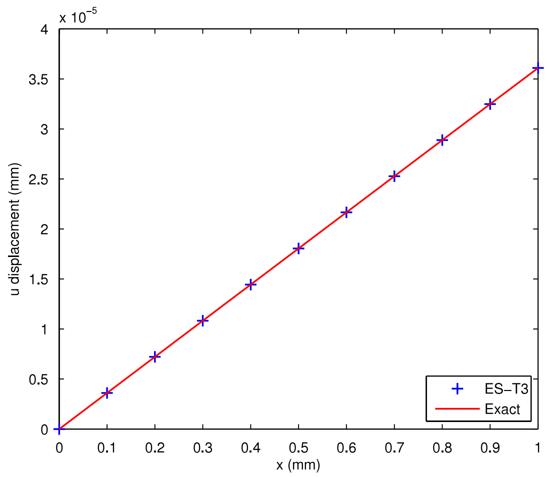

Figure 4. Variation of horizontal displacement u at the central line ($y = 0$) of the singer-player piezoelectric strip.

to the edges of the strip:

$$
\begin{aligned}
&\phi_{,y}(x, y = \pm h) = 0, && T_{yy}(x, y = \pm h) = \sigma_0,\\
&T_{xy}(x = L, y) = 0 && T_{xy}(x, y = \pm h) = 0,\\
&\phi(x = L, y) = -V_0, && T_{xx}(x = L, y) = 0\\
&\phi(x = 0, y) = +V_0, && u(x = 0, y) = 0,\\
&v(x = 0, y = 0) = 0.
\end{aligned}
\tag{48}
$$

The analytical solution for this problem is given by Ohs *et al* [14]:

$$
u = s_{13}\sigma_0 x, \qquad v = \frac{d_{15}V_0 x}{h} + s_{33}\sigma_0 y,
\qquad \phi = V_0\left(1 - 2\frac{x}{L}\right).
\tag{49}
$$

The calculated results are depicted in figures 4–6. It is seen that the results of the ES-T3 element match the exact solutions. This also means that the ES-T3 element can reproduce the linear behavior of the analytical solution.

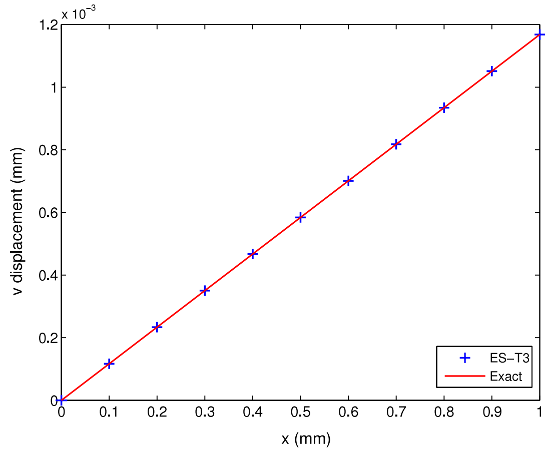

Figure 5. Variation of vertical displacement v at the central line ($y = 0$) of the singer-player piezoelectric strip.

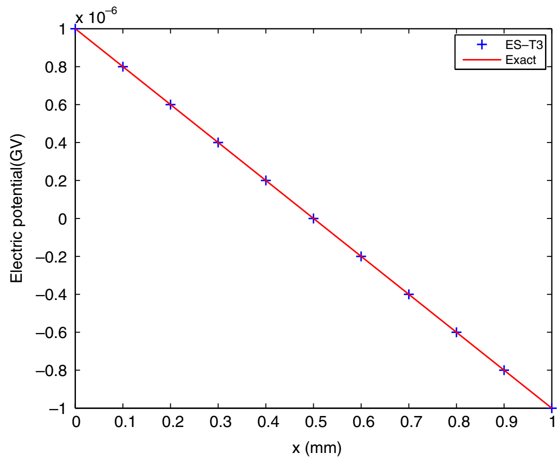

Figure 6. Variation of electric potential ϕ at the central line ($y = 0$) of the singer-player piezoelectric strip.

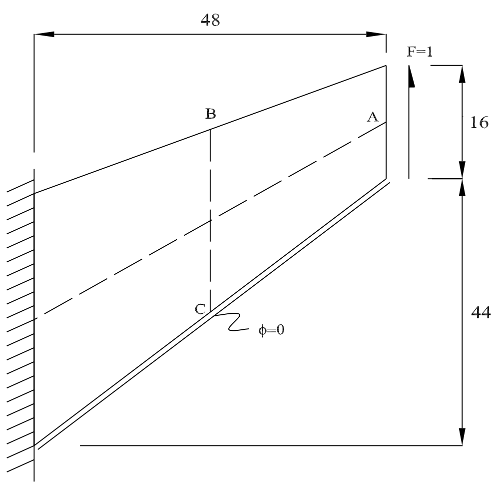

Figure 7. Cook's membrane.

4.4. Cook's membrane

This benchmark problem, shown in figure 7, refers to a clamped tapered panel subjected to a distributed tip load,

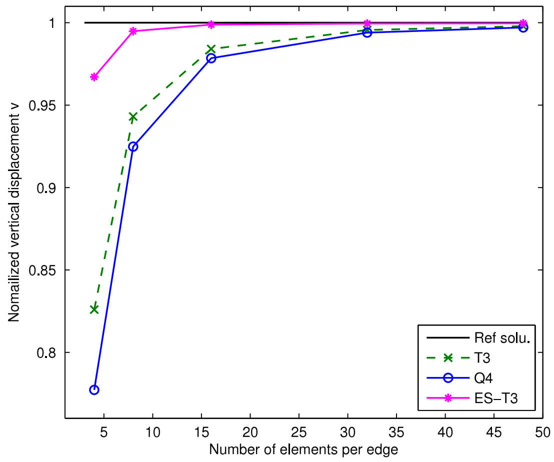

Figure 8. Convergence of vertical displacement at point A of Cook's membrane.

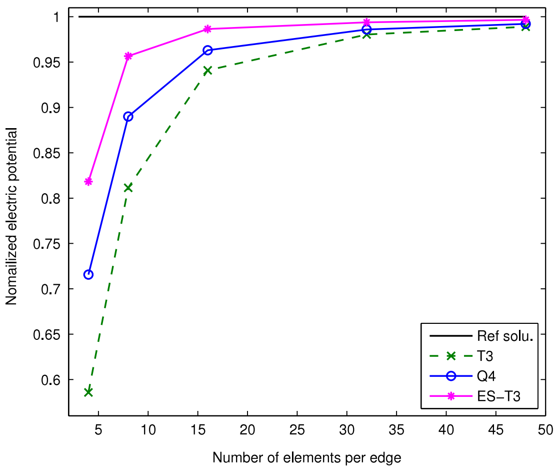

Figure 9. Convergence of electric potential at point A of Cook's membrane.

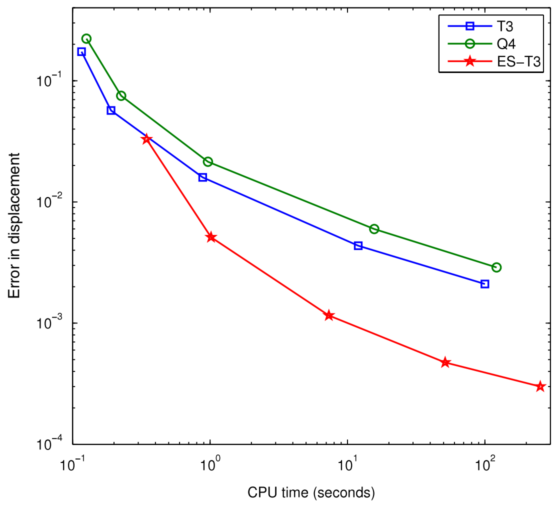

Figure 10. Comparison of the computational efficiency in displacement error of Cook's membrane.

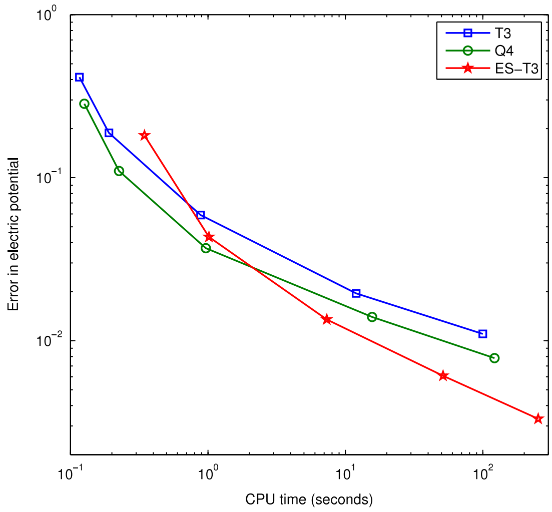

Figure 11. Comparison of the computational efficiency in electric potential error of Cook's membrane.

resulting in deformation dominated by a bending response. The PZT4 material is used. The mechanical boundary conditions are similar to the popular Cook's membrane [29]. The boundary condition of the lower surface is prescribed by zero voltage (0 V). The analytical solution of the problem is unknown. The reference value of the vertical displacement and the electric potential at the center tip (A) is 2.109×10^{-4} mm and 1.732×10^{-8} GV [13].

The convergence of the vertical displacement at point A is illustrated in figure 8. It is shown that the ES-T3 element achieves the best prediction for vertical displacement at point A. Figure 9 presents results of the electric potential at point A. It is clear that the ES-T3 element is superior to the T3 and Q4 elements.

Now we mention the computational efficiency of the present method compared with FEM models. The program is compiled by a personal computer with Intel(R) Core (TM) 2 Duo CPU—2 GHz and RAM—2 GB. The computational cost is to set up the global stiffness matrix and to solve the algebraic equations. Owing to the establishment of the smoothed strain (27) and the smoothed electric field (28), no additional degrees of freedom are required in the ES-FEM. Figures 10 and 11 illustrate the errors in vertical displacement and electric potential at point A against the CPU time (seconds) for Cook's membrane problem. It is observed that the 'overhead' computation time of the ES-T3 is little longer than those of the Q4 and the T3, due to the additional time required for the additional operations related to the stiffness matrix. However, in terms of the computational efficiency (computation time for the same accuracy) measured in both displacement and electric potential errors, the ES-T3 is the more effective. More details for the convenience of ES-T3 can be found in the previous work in [27].

4.5. MEMs device

The purpose of this problem is to simulate the linear tilt angle of the reflected light through a mirror of an MEMs device. The device is constructed from two parallel bimorphs made of

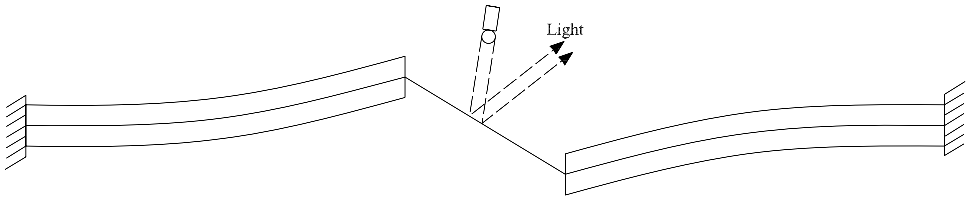

Figure 12. Bimorph MEMs device.

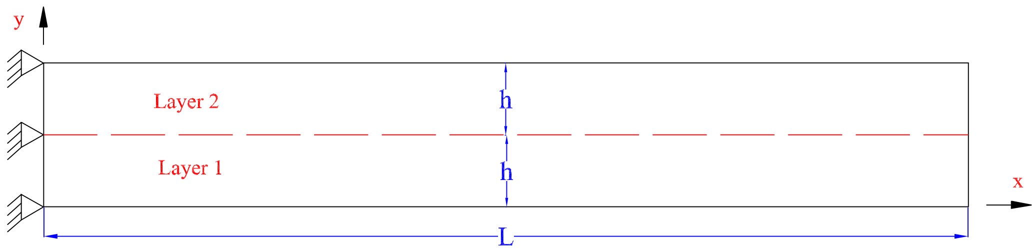

Figure 13. Parallel bimorph geometry.

PVDF material connected by a mirror as shown in figure 12. Each bimorph with length $L = 10$ μm and height $H = 1$ μm is assumed. The bimorph beam is divided into top and bottom layers as shown in figure 13.

The following boundary conditions are applied to layer 1 of the bimorph beam:

$$\begin{gathered}
\phi^{(1)}(x, y=0) = V, \qquad T_{yy}^{(1)}(x, y=0) = 0, \\
T_{xy}^{(1)}(x, y=0) = 0 \\
\phi^{(1)}(x, y=h) = 0, \qquad T_{yy}^{(1)}(x, y=h) = T_{yy}^{(2)}(x, y=h) \\
T_{xy}^{(1)}(x, y=h) = T_{xy}^{(2)}(x, y=h) \\
\phi_{,x}^{(1)}(x=0, y) = 0, \qquad u^{(1)}(x=0, y) = 0, \\
v^{(1)}(x=0, y) = 0 \\
\phi_{,x}^{(1)}(x=L, y) = 0, \qquad T_{xx}^{(1)}(x=L, y) = 0, \\
T_{xy}^{(1)}(x=L, y) = 0.
\end{gathered} \tag{50}$$

Boundary conditions for layer 2 were

$$\begin{gathered}
\phi^{(2)}(x, y=h) = \phi^{(1)}(x, y=h), \\
u^{(2)}(x, y=h) = u^{(1)}(x, y=h) \\
v^{(2)}(x, y=h) = v^{(1)}(x, y=h), \\
\phi^{(2)}(x, y=2h) = V \\
T_{yy}^{(2)}(x, y=2h) = 0, \qquad T_{xy}^{(2)}(x, y=2h) = 0 \\
\phi_{,x}^{(2)}(x=0, y) = 0, \qquad u^{(2)}(x=0, y) = 0, \\
v^{(2)}(x=0, y) = 0 \qquad \phi_{,x}^{(2)}(x=L, y) = 0, \\
T_{xx}^{(2)}(x=L, y) = 0, \qquad T_{xy}^{(2)}(x=L, y) = 0.
\end{gathered} \tag{51}$$

The centers of bimorphs are connected by a 1 μm long mirror. Linear elastic is assumed to the mirror. When a voltage is applied, the bimorphs vertically displace in opposite directions and rotate the mirror with the tilt angle. As a result, the direction of the reflected light can change when the various voltages are applied.

Table 2. Tip deflections (μm).

Applied voltage (V)	T3	Q4	ES-T3	Ref [14]
1.00	0.004 794	0.004 866	0.004 808	0.004 936
2.00	0.009 588	0.009 731	0.009 614	0.009 872
5.00	0.023 971	0.024 328	0.024 034	0.024 681
10.00	0.047 942	0.048 655	0.048 068	0.049 362
15.00	0.071 913	0.072 983	0.072 102	0.074 043
20.00	0.095 884	0.097 310	0.096 136	0.098 724
25.00	0.119 855	0.121 638	0.120 169	0.123 405
50.00	0.239 710	0.243 276	0.241 339	0.246 811

Note that the analytical solution of this problem is not available. Therefore, similar to the analysis given in [14], a mesh (80 × 20) of 1701 nodes is used. The tip displacements of the bimorphs using the FEM and ES-FEM are computed for several voltages. From the tip displacement, the tilt angle of the mirror is found and compared to the reference result in [14]. The tilt angle of the mirror could be calculated by normal deflection of the beam at the point connection between mirror and beam in which the horizontal displacement of this point is supposed to be zero.

The results of the T3, Q4 and ES-T3 are given in table 2. The tilt angle is described in figure 14. Similar to the meshless point collocation method (PCM) [14], it is also found that the tip displacements of the bimorphs and the tilt angle of the mirror for both FEM and ES-FEM models vary linearly with applied voltages.

Note that the displacement of the ES-T3 is larger than that of the T3 because the model of the ES-T3 is softer than that of the T3 element. However, for this problem, ES-T3 solutions are slightly stiffer than those of Q4 and the meshless point collocation method (PCM). This can be due to the shear

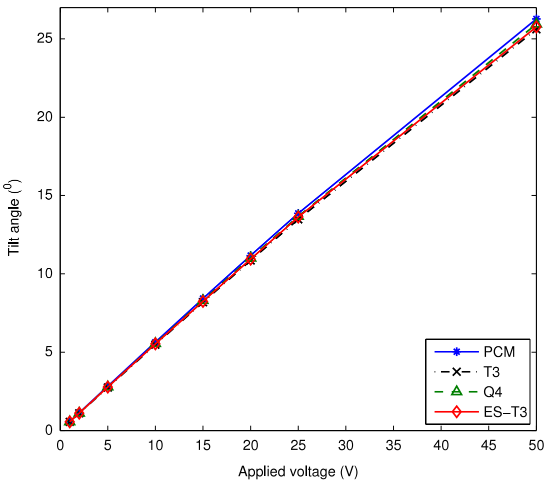

Figure 14. Tilt angle of mirror in the bimorph MEMs device.

Table 3. Eigenvalues (kHz) using 175 nodes (272 triangular elements).

Element type	Mode 1	Mode 2	Mode 3	Mode 4	Mode 5
T3	19.98 (7.42%)	43.31 (24.01%)	62.78 (15.83%)	67.78 (7.08%)	94.23 (6.12%)
Q4	19.7 (5.91%)	42.9 (21.19%)	61.1 (12.73%)	66.7 (5.37%)	92.2 (3.83%)
ES-T3	18.74 (0.75%)	41.74 (17.91%)	59.21 (9.24%)	65.23 (3.05%)	89.85 (1.18%)
Experi-mental [31]	18.6	35.4	54.2	63.3	88.8

effect generated from the present element when it is used to model thin bimorph beams [14]. Therefore, a finer mesh or an interpolation function of higher-order approximation is more appropriate to provide the same accuracy as the PCM.

4.6. Eigenvalue analysis of a piezoelectric transducer

This example performs an eigenvalue analysis of a cylindrical transducer using a piezoelectric material PZT4 wall with brass end caps as shown in figure 15. On inner and outer surfaces of the structure, the electrode is imposed. This illustration is a typical problem given in section 6.1.1 in the ABAQUS manual [30]. This problem is also identical to the one resulting experimentally in Mercer *et al* [31]. The transducer is modeled as an axisymmetric problem and the discretization with quadrilateral and triangular elements is illustrated by figure 16. Homogeneous constraints of the potentials on the inside surface are restrained. The frequencies correspond to those for anti-resonance. The ES-FEM approach is now applied to analyze the eigenvalues of the transducer. For comparison, we use uniform meshes of 136 rectangular elements (272 triangles) as shown in figure 16. Table 3 shows the first five frequencies, and the relative error percentages compared with experimental results are given in parentheses. Their corresponding eigenmode shapes are plotted in figure 17.

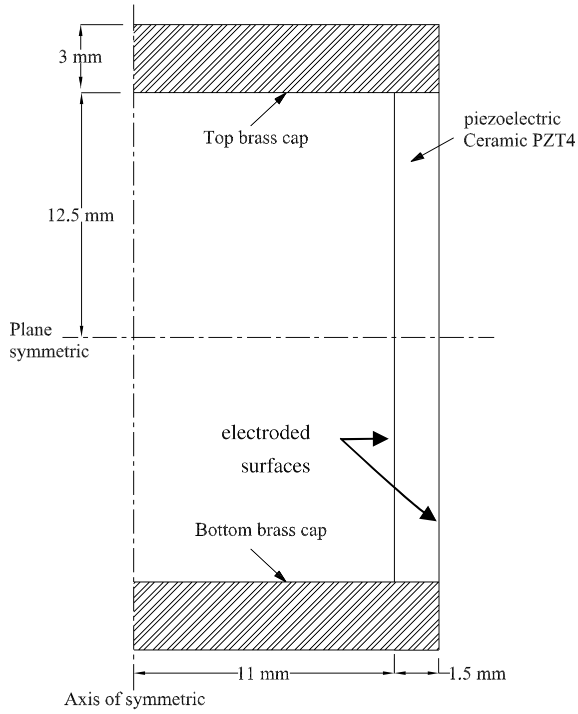

Figure 15. Schematic presentation of a transducer.

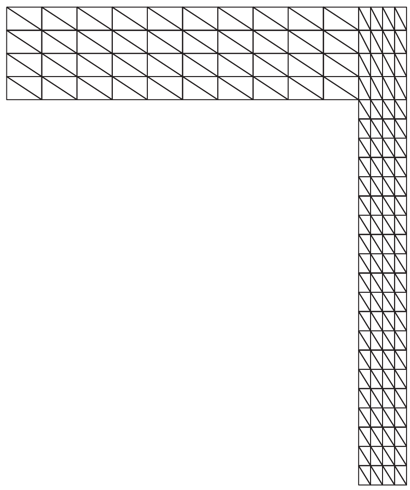

Figure 16. Domain discretization of the transducer using 136 rectangular elements (272 triangles).

It can be seen that these eigenmode shapes are identical to those described in the ABAQUS manual [30].

From table 3, it is observed that the ES-T3 gives a good agreement with the experimental results from Mercer *et al* [31]. The relative error percentage corresponding to each mode of ES-T3 is smaller than that of T3 and Q4 elements. This means that the eigenvalues of the ES-T3 are better than those of standard finite elements.

5. Conclusions

An edge-based smoothed finite element method using a triangular mesh for analyses of two-dimensional piezoelectric

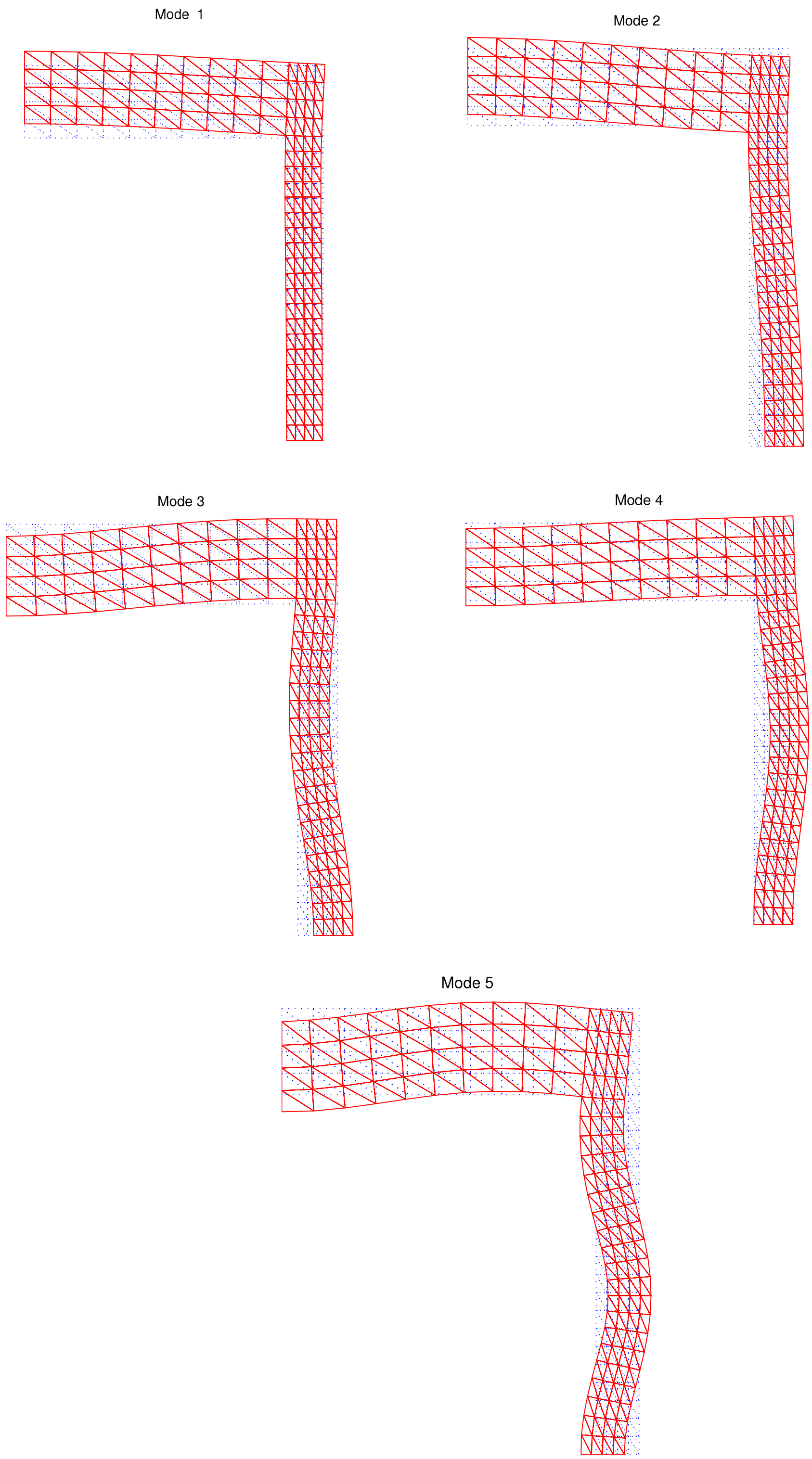

Figure 17. Eigenmodes for the piezoelectric transducer by the ES-T3.

structures is further studied. In the present method, the displacements and electric potentials are approximated as in the standard FEM, but the mechanical strains and the electric displacements are smoothed over the smoothing domain associated with the edges of the triangles. As a result, the coupled stiffness mechanical and electrical matrices based on these smoothed fields are simply obtained. More importantly, the ES-FEM only uses triangular meshes with DOF at vertex nodes and no additional degrees of freedom are required. The present method passes the patch test for plane piezoelectric problem. The obtained results of the ES-FEM are in a good agreement with analytical solution as well as experimental results. The ES-T3 element is much more reliable and accurate than the T3 and is often found to be even more accurate than the Q4 element for tested static problems and for eigenvalue analysis of the transducer. Furthermore, the ES-FEM is very easy to implement in a finite element program using triangular meshes that can be generated with ease for complicated problem domains.

References

[1] Benjeddou A 2000 Advances in piezoelectric finite element modeling of adaptive structural elements: a survey *Comput. Struct.* **76** 347–63
[2] Allik H and Hughes T J R 1970 Finite element method for piezo-electric vibration *Int. J. Numer. Methods Eng.* **2** 151–7
[3] Tzou H S and Tseng C I 1990 Distributed piezoelectric sensor/actuator design for dynamic measurement/control of distributed parameter systems: a finite element approach *J. Sound Vib.* **138** 17–34
[4] Cannarozzi A A and Ubertini F 2001 Some hybrid variational methods for linear electroelasticity problems *Int. J. Solids Struct.* **38** 2573–96
[5] Sze K Y and Pan Y S 1999 Hybrid finite element models for piezoelectric materials *J. Sound Vib.* **226** 519–47
[6] Sze K Y, Yao L Q and Yi S 2000 A hybrid stress ANS solid-shell element and its generalization for smart structure modelling. Part II—smart structure modelling *Int. J. Numer. Methods Eng.* **48** 565–82
[7] Sze K Y and Yao L Q 2000 Modelling smart structures with segmented piezoelectric sensors and actuators *J. Sound Vib.* **235** 495–20
[8] Wu C C, Sze K Y and Huang Y Q 2001 Numerical solutions on fracture of piezoelectric materials by hybrid element *Int. J. Solids Struct.* **38** 4315–29
[9] Sze K Y, Yang X M and Yao L Q 2004 Stabilized plane and axisymmetric piezoelectric finite element models *Finite Elem. Anal. Des.* **40** 1105–22
[10] Bergan P G and Felippa C A 1985 A triangular membrane element with rotational degrees of freedom *Comput. Methods Appl. Mech. Eng.* **50** 25–69
[11] Sze K Y, Wanji C and Cheung Y K 1992 An efficient quadrilateral plane element with drilling degrees of freedom using orthogonal stress modes *Comput. Struct.* **42** 695–705
[12] Groenwold A A and Stander N 1998 A 24 d.o.f. 4-node flat shell finite element for general unsymmetric orthotropic layered composites *Eng. Comput.* **15** 518–43
[13] Long C S, Loveday P W and Groenwold A A 2006 Planar four node piezoelectric with drilling degrees of freedom *Int. J. Numer. Methods Eng.* **65** 1802–30
[14] Ohs R R and Aluru N R 2001 Meshless analysis of piezoelectric devices *Comput. Mech.* **27** 23–36
[15] Liu G R, Dai K Y, Lim K M and Gu Y T 2002 A point interpolation mesh free method for static and frequency analysis of two-dimensional piezoelectric structures *Comput. Mech.* **29** 510–9
[16] Liu G R, Dai K Y, Lim K M and Gu Y T 2003 A radial point interpolation method for simulation of two-dimensional piezoelectric structures *Smart Mater. Struct.* **12** 171–80
[17] Liu G R, Dai K Y and Nguyen T T 2007 A smoothed finite element method for mechanics problems *Comput. Mech.* **39** 859–77
[18] Liu G R, Nguyen T T, Dai K Y and Lam K Y 2007 Theoretical aspects of the smoothed finite element method (SFEM) *Int. J. Numer. Methods Eng.* **71** 902–30
[19] Nguyen T T, Liu G R, Dai K Y and Lam K Y 2007 Selective smoothed finite element method *Tsinghua Sci. Technol.* **12** 497–508
[20] Chen J S, Wu C T, Yoon S and You Y 2001 A stabilized conforming nodal integration for Galerkin mesh-free methods *Int. J. Numer. Methods Eng.* **50** 435–66
[21] Dai K Y, Liu G R and Nguyen T T 2007 An n-sided polygonal smoothed finite element method (nSFEM) for solid mechanics *Finite Elem. Anal. Des.* **43** 847–60
[22] Dai K Y and Liu G R 2007 Free and forced vibration analysis using the smoothed finite element method (SFEM) *J. Sound Vib.* **301** 803–20
[23] Nguyen-Xuan H, Rabczuk T, Bordas S and Debongnie J F 2008 A smoothed finite element method for plate analysis *Comput. Methods Appl. Mech. Eng.* **197** 1184–203
[24] Nguyen-Thanh N, Rabczuk T, Nguyen-Xuan H and Bordas S 2008 A smoothed finite element method for shell analysis *Comput. Methods Appl. Mech. Eng.* **198** 165–77
[25] Nguyen-Van H, Mai-Duy N and Tran-Cong T 2008 A smoothed four-node piezoelectric element for analysis of two-dimensional smart structures *Comput. Model. Eng. Sci.* **23** 209–22
[26] Liu G R, Nguyen-Thoi T, Nguyen-Xuan H and Lam K Y 2009 A node-based smoothed finite element method (NS-FEM) for upper bound solutions to solid mechanics problems *Comput. Struct.* **87** 14–26
[27] Liu G R, Nguyen-Thoi T and Lam K Y 2009 An edge-based smoothed finite element method (ES-FEM) for static, free and force vibration analyses of solids *J. Sound Vib.* **320** 1100–30
[28] Nguyen-Thoi T, Liu G R and Lam K Y 2009 A face-based smoothed finite element method (FS-FEM) for 3D linear and nonlinear solid mechanics problems using 4-node tetrahedral elements *Int. J. Numer. Methods Eng.* **78** 324–53
[29] Cook R 1974 Improved two–dimensional finite element *J. Struct. Div. ASCE* **100** (ST6) 1851–63
[30] *ABAQUS/Standard Example Problems Manual* 2006 Version 6.6 (Hibbitt: Karlsson and Sorensen Inc.) section 6.1.1
[31] Mercer C D, Reddy B D and Eve R A 1987 Finite element method for piezoelectric media *Applied Mechanics Research Unit Technical Report* No 92 University of Cape Town/CSIR